



## Engineering behavior influence of basaltic rocks on the adsorption of heavy metal ions

Nabila S. Ammar<sup>a,\*</sup>, Ali I.M. Ismail<sup>b</sup>, Ola I. El-Shafey<sup>c</sup>

<sup>a</sup>Water Pollution Research Department, National Research Centre, El-Behooth Street, Dokki, Giza 12622, Egypt, Tel. +002 0128 455 7301; Fax: +0020 2 33371479; email: [nabilaammar@yahoo.com](mailto:nabilaammar@yahoo.com)

<sup>b</sup>Geological Sciences Department, National Research Centre, El-Behooth Street, Dokki, Giza 12622, Egypt, email: [ali\\_ismail\\_2000@yahoo.com](mailto:ali_ismail_2000@yahoo.com)

<sup>c</sup>Physical Chemistry Department, National Research Centre, El-Behooth Street, Dokki, Giza 12622, Egypt, email: [olalolo2004@yahoo.com](mailto:olalolo2004@yahoo.com)

Received 1 April 2014; Accepted 9 December 2014

---

### ABSTRACT

Basaltic rocks obtained from Qusier area, south Eastern Desert, Egypt showed to be effective in removing heavy metals from aqueous solution. According to mechanical and engineering scheme, the basaltic rocks were classified into basalt weathering grade I (BWGI) and basalt weathering grade II (BWGII). The adsorption of  $Pb^{2+}$  using BWGI and BWGII from aqueous solution was studied under various conditions. The uptake of  $Pb^{2+}$  was rapid with maximum adsorption within 90 min for BWGI and 60 min for BWGII. The kinetic of the  $Pb^{2+}$  adsorption was studied using pseudo-first-order, pseudo-second-order, Elovich and intraparticle diffusion models. The kinetics data showed that the adsorption of  $Pb^{2+}$  onto basalt proceeds according to the pseudo-second-order model. The results obtained from adsorption isotherm indicated that the maximum adsorption capacities of  $Pb^{2+}$  were 15.92 and 23.31 mg/g by BWGI and BWGII, respectively. The mean sorption energy ( $E$ ) obtained from Dubinin-Radushkevich isotherm model indicated that, the adsorption process takes place chemically and the reaction is endothermic. The results suggested that natural basalt, especially, BWGII is suitable as an adsorbent material for adsorption of  $Pb^{2+}$  from aqueous solutions.

*Keywords:* Engineering behavior of basalts; Mechanical classification of basalts; Grade of weathering; Adsorption; Kinetic and isotherm models

---

### 1. Introduction

The earth's surface contains 8.5% of the rocks that are basaltic [1]. Alteration of highly reactive and easy weatherable basalts has a marked contribution to the global chemical budgets of both the atmosphere and hydrosphere. Weathering is a slow process that affects

the rocks and the stability of structures in two ways; one is short term and the other is long term [2]. Under the atmospheric conditions, the changes that occur in the mechanical and physical properties of the rocks are due to weathering and are controlled by their chemical, mineralogical as well as textural composition. Different compositions of rocks could make different degrees of weathering under the same

---

\*Corresponding author.

conditions and show different properties. Different mechanical and index tests have been used to characterize the degree of weathering [3–6].

The presence of heavy metals in wastes and surface water is becoming a severe environmental problem and because of their non-biodegradability, they can accumulate in the food chain posing a significant danger to human health [7]. Lead (Pb), in particular, is one of the most common environmental contaminants due to its wide use in petroleum, mining, paint, pigments, ceramics, and weapons industries. Many techniques such as adsorption, chemical oxidation, precipitation, solvent extraction, ion exchange, membrane processes, and reverse osmosis have been developed for metal ions removal from aqueous solutions [8]. Among them, adsorption technology is the most promising process involved in the removal of toxic metals from industrial waste streams and natural waters with the selection of a suitable adsorbent [7,9].

The main objective of this study was to estimate the applicability of natural basalt at different grade of weathering in removal of  $Pb^{2+}$  from aqueous solutions by batch adsorption process.

## 2. Materials and methods

### 2.1. Characterization of basaltic rocks

This study has been investigated on the removal efficiency of  $Pb^{2+}$  from synthetic aqueous solution using basaltic rocks. Two types of basaltic rocks, basalt weathering grade I (BWGI) and basalt weathering grade II (BWGII), were discriminated by the engineering characteristics and chemical analysis. Various tests had been performed to determine chemical and physical properties of the adsorbents (BWGI and BWGII). For example, the uniaxial compressive strength was considered as the most reliable index for strength and deformability estimation of rocks. The weathering results cause an immediate and significant reduction in the compressive strength of rocks [10]. Gupta and Rao [11] found that the uniaxial compressive strength decreases with increasing weathering stage. Compressive and tensile strength (TS) has been used to differentiate between the basaltic rocks according to the weathering grade.

The grain size and texture have more importance in controlling the TS rather than compressive strength.

X-ray fluorescence spectrometry was applied to estimate the chemical constituents and petrological classification of the basaltic rocks. The X-ray powder diffractograms were carried out to determine the mineral constituent of the samples. Scanning electron microscope (SEM) photographs and a nitrogen

adsorption system (Quantachrome NOVA Automated Gas Sorption System) were employed to measure adsorption–desorption isotherms at  $-196^{\circ}C$ .

### 2.2. Batch adsorption tests

$Pb(NO_3)_2$  of analytical grade from Merck was used in the preparation of the stock standard solution (1,000 mg/L). The working solution was prepared by diluting the stock solution to the appropriate volume. The pH of the aqueous solution of metal ions as prepared was  $5.5 \pm 0.1$ . The concentrations of metal in all samples were determined according to standard method [12] using an atomic absorption spectrometer {Varian Spectra (220)} with graphite furnace accessory and equipped with deuterium arc background corrector. The precision of the metal measurement was determined by analyzing (in triplicate) the metal concentration of all samples.

### 2.3. Adsorption by basaltic materials

#### 2.3.1. Comparison of BWGI and BWGII

To assess the ability of the BWGI and BWGII for adsorbing the metal ions, metal uptake capacities were tested. Metal uptake capacities were determined by shaking 0.5 g of BWGI and BWGII with a synthetic solution of  $Pb^{2+}$  (50 mg/L) in a mechanical shaker at 200 rpm for 2 h. The pH value of  $5.0 \pm 0.1$  was maintained throughout the experiment by adding 0.1 N NaOH or HCl. At this pH value, there would be little competition between metal ions and protons compared to lower pH values, which lead to high metal uptake [13].

The metal ion concentrations, retained in the adsorbed phase at (mg/g), were calculated using the following equation:

$$q_t = \frac{(C_0 - C_t)V}{M} \quad (1)$$

where  $C_0$  (mg/L) is the initial metal ion concentration,  $C_t$  (mg/L) is the equilibrium concentration of metal ions in aqueous solution,  $V$  (L) is the volume of solution,  $M$  (g) is the mass of the adsorbent, and  $q_t$  (mg/g) is the calculated metal ion adsorption amount onto basalt.

#### 2.3.2. The effect of initial pH

The protonation of the functional groups on the adsorbent surface and ionization degrees of the

adsorbates depend on the initial pH of the aqueous solution. Therefore, the effect of initial pH on the removal of  $Pb^{2+}$  was studied with an initial metal ion concentration of 50 mg/L and basalt dose of 5 g/L by varying the pH of the solutions over the range of 2–5.5.

The removal efficiency (%  $R_E$ ) of the metal ion was calculated using the following equation:

$$R_E \% = \frac{(C_0 - C_e) \times 100}{C_0} \quad (2)$$

where  $C_0$  and  $C_e$  are the initial and equilibrium liquid-phase concentrations of  $Pb^{2+}$  in aqueous solution (mg/L).

### 2.3.3. Effect of contact time and adsorption kinetics

The time-dependent behavior of  $Pb^{2+}$  adsorption onto both BWGI and BWGII (5 g/L) was evaluated for different equilibrium time intervals from 5 to 120 min using an initial  $Pb^{2+}$  concentration of 50 mg/L at room temperature and at optimum pH ( $5.0 \pm 0.1$ ).

### 2.3.4. Effect of weathering basalt dose

A series of experiments were conducted using different doses of weathering basalt in the range of 1–10 g/L with an initial metal ion concentration of 50 mg/L at an optimum contact time and pH ( $5.0 \pm 0.1$ ), respectively.

### 2.3.5. Effect of initial metal ion concentrations and adsorption isotherm

Adsorption isotherm of  $Pb^{2+}$  onto BWGI and BWGII was investigated at the optimum conditions using batch experiments. Adsorption isotherm models used in this study were Langmuir, Freundlich, and Dubinin–Radushkevich (D–R) isotherms. They differ in their assumption, shape of the isotherm, and the nature of the adsorbent surface.

## 3. Results and discussion

### 3.1. Characterization of basalt

#### 3.1.1. Chemical and engineering analysis

Two different grades of weathering basaltic rocks were used in this study. Some tests had been performed to determine basalt properties. The chemical analysis (Table 2) confirmed that the samples are

plotted in basalt field (Fig. 1) according to Cox et al. [14]. The engineering tests were performed in different weathering rates. The engineering parameter values of the rocks in different weathering stages were determined to investigate the effect of weathering degree on the engineering behavior of rocks. The values of the unified compression strength (UCS) and TS decrease as the weathering increase, whereas water absorption increases with increasing the weathering rate as shown in Table 1. The engineering parameter values showed that as the weathering increases, the strength and durability behavior decreases. Finally, results of this study specified that the more weathering basalt has good quality for adsorption.

According to Verhoef and Van De Wall [15] and IPT (Instituto de Pesquisas Tecnológicas do Estado de São Paulo) [16], the highest weathering grade of the samples under study is classified as a good quality to the adsorption process (Table 3).

#### 3.1.2. X-ray diffraction analysis

The mineralogical compositions of BWGI and BWGII rocks were determined by X-Ray powder diffraction patterns. Fig. 1 shows that Basaltic rocks are composed of plagioclase, hornblende, pyroxene (augite), and chlorite. This finding shows that the increasing of weathering process leads to an increase in the degree of alteration minerals.

The alteration plagioclase and pyroxene increases from weathering grade BWGI to BWGII (Fig. 2).

#### 3.1.3. Scanning electron microscope (SEM)

Fig. 3 shows the morphology of BWGI and BWGII rocks that taken at 13,000 times magnification. From Fig. 3, it can be seen that the surface of basalts is heterogeneous which are composed of irregular and porous particles with size ranged between 2–4  $\mu\text{m}$ .

#### 3.1.4. Effect of weathering process on surface properties of basalt

Nitrogen adsorption–desorption isotherms at  $-196^\circ\text{C}$  were studied for BWGI and BWGII rocks. The specific surface area  $S_{\text{BET}}$ , total pore volume  $V_P$ , and mean pore radius  $\bar{r}$  are listed in Table 4. Table 4 shows that the  $S_{\text{BET}}$  surface area drastically increases with increasing total pore volume, while the mean pore radius considerably decreases with the weathering process. This significant increase in  $S_{\text{BET}}$  due to weathering process could be attributed to pore widening.

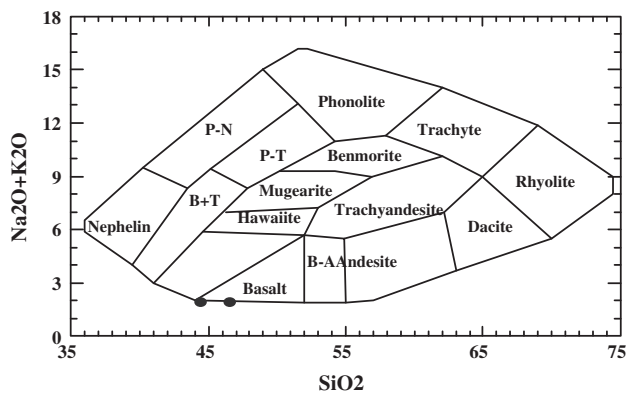


Fig. 1. Schematic diagrams for the rock under study.

Table 1

Engineering parameters of basaltic samples at different grade of weathering

Compound	Water absorption (%)	UCS (Mpa)	TS (Mpa)
BWGI	0.53	85.23	47.58
BWGII	0.86	70.29	39.21

### 3.2. Comparison of BWGI and BWGII

The results showed that the adsorption capacities of  $Pb^{2+}$  onto both BWGI and BWGII were 9.37 and 9.82 mg/g, respectively. This means that the uptake capacity of  $Pb^{2+}$  using BWGII was slightly more than BWGI because surface area of BWGII (38.57  $m^2/g$ ) is more than BWGI (28.58  $m^2/g$ ), which is due to the weathering process.

Table 2

Chemical composition of basaltic samples

Compound formula	SiO <sub>2</sub>	TiO <sub>2</sub>	Al <sub>2</sub> O <sub>3</sub>	Fe <sub>2</sub> O <sub>3</sub>	MnO	MgO	CaO	Na <sub>2</sub> O	K <sub>2</sub> O	P <sub>2</sub> O <sub>5</sub>	Cl	SO <sub>3</sub>	LOI
BWGI	44.49	1.85	9.74	11.24	0.18	4.22	11.87	1.60	0.29	0.15	0.01	0.10	13.74
BWGII	46.60	1.80	9.87	11.23	0.20	5.35	12.74	1.58	0.31	0.16	<0.01	0.08	9.57

Table 3

Guide to rock durability from test results [15,16]

Compound	Test	Excellent quality	Good quality	Reasonable quality	Bad quality
BWGI	UCS (MPa)	>200	200–100	100–50	>50
BWGII	Water absorption (%)	<0.5	0.5–2.0	2.0–6.0	>6.0

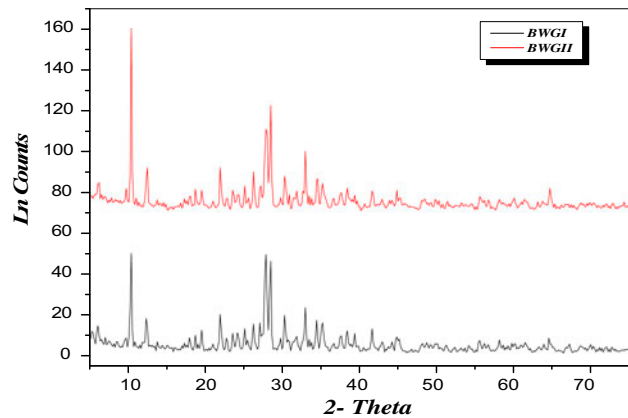


Fig. 2. XRD of BWGI and BWGII.

### 3.3. Effect of initial pH

The effect of pH on  $Pb^{2+}$  adsorption onto both BWGI and BWGII was studied in the pH range between 2 and 5.5, where the experiments were not conducted beyond pH 5.5 to avoid the precipitation of metal ions [17]. The results showed that the removal percentage of  $Pb^{2+}$  increased from 34.1 to 93.8% using BWGI and from 40.2 to 98.2% using BWGII for pH 2–4.5 and remains almost constant for pH 4.5–5.5. At low pH, surface active sites of BWGI and BWGII may become positively charged leading to increase the competition between  $H^+$  and  $Pb^{2+}$  for available adsorption sites. However, as pH increases, this competition decreases as these surface active sites become more negatively charged, which enhances the adsorption of the positively charged metal ions through electrostatic force of attraction [18,19].

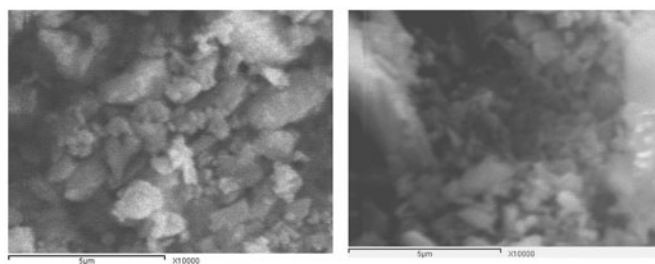


Fig. 3. SEM images of BWGI and BWGII at magnification 13,000×.

Table 4  
Specific surface area, total pore volume and mean pore radius of BWGI and BWGII clays

Sample	$S_{BET}$	$V_p$ (ccg)	$r^-$ (Å)
BWGI	28.57	$9.97 \times 10^{-3}$	13.96
BWGII	38.57	$1.2 \times 10^{-2}$	13.3

### 3.4. Effect of contact time

The effect of contact time was studied at different time in the range 5–120 min using 50 mg/L of  $Pb^{2+}$  solution, 5 g/L of both BWGI and BWGII at optimum pH, and at ambient temperature ( $25 \pm 1^\circ C$ ). The data in Fig. 4 show that the removal percentage of  $Pb^{2+}$  increases with increasing contact time, and remained nearly constant after equilibrium. Therefore, the equilibrium time was attained within 60 min for BWGII, and more than 60 min for BWGI.

### 3.5. Adsorption kinetics

The study of adsorption dynamics describes the solute uptake rate and this rate controls the habitation time of adsorbate uptake at the solid–solution

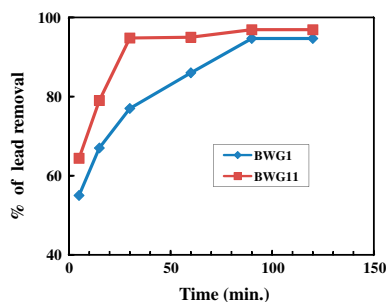


Fig. 4. Effect of contact time on adsorption of  $Pb^{2+}$  using BWGI and BWGII (volume of solution = 100 mL, concentration of metal ions = 50 mg/L, dose of adsorbents = 0.5 g and pH  $5.0 \pm 0.1$ ).

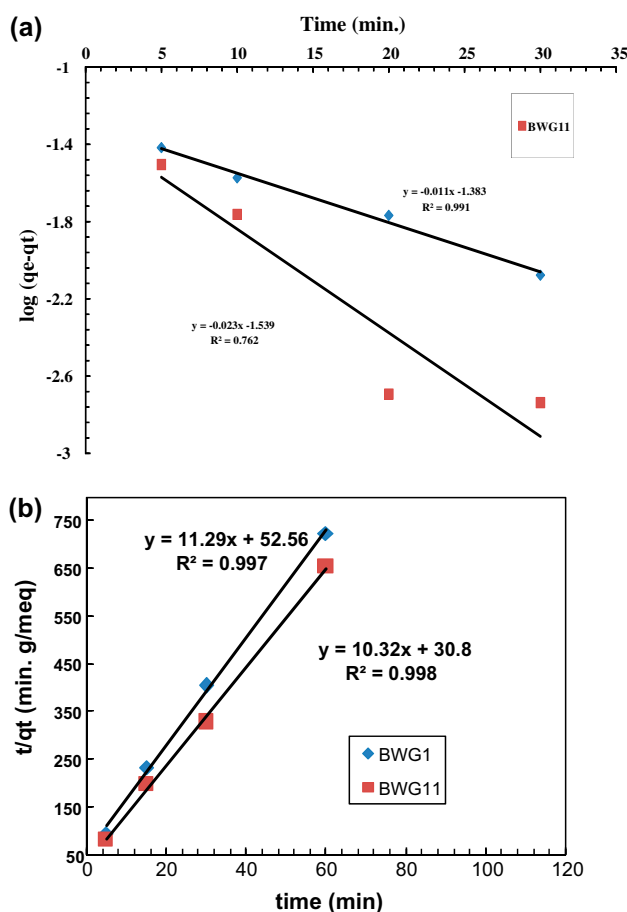


Fig. 5. (a) Pseudo-first-order kinetics for  $Pb^{2+}$  adsorption onto BWGI and BWGII and (b) Pseudo-second-order kinetics for  $Pb^{2+}$  adsorption onto BWGI and BWGII.

interface. In addition, sorption kinetics shows a large dependence on the physical and/or chemical characteristics of the adsorbent material. Therefore, different models such as pseudo-first-order, pseudo-second-order, Elovich kinetic, and intraparticle diffusion models have been used to study the mechanism of the adsorption process.

### 3.5.1. Pseudo-first-order or kinetic model

The pseudo-first-order is generally proposed by Lagergren [20] as follows:

$$\frac{dq}{dt} = k_1(q_e - q_m) \frac{dq}{dt} \quad (3)$$

Integrating Eq. (3) with respect to integration conditions  $q = 0$  to  $q = q_t$  at  $t = 0$  to  $t = t$ , the kinetic rate expression becomes:

$$\text{Log}(q_e - q_t) = \text{Log}q_e - \frac{k_1 t}{2.303} \quad (4)$$

where  $q_e$  and  $q_t$  (mg/g): are the amounts of  $\text{Pb}^{2+}$  adsorbed (mg/g) at equilibrium and at time  $t$  (min), respectively and  $k_1$  is the adsorption rate constant ( $\text{min}^{-1}$ ).

From the plots of  $\log(q_e - q_t)$  vs.  $t$ , the values of  $k_1$  and  $q_e$  are calculated from the slope and intercept as shown in Fig. 5(a). The adsorption first-order rate constants were found to be 0.0253 and 0.0532  $\text{min}^{-1}$  and the correlation coefficient  $R^2$  values were 0.9919 and 0.7626 for adsorption  $\text{Pb}^{2+}$  onto both BWGI and BWGII, respectively. If the adsorption process can be described by the pseudo-first-order equation, there should be a good linear relationship between  $\log(q_e - q_t)$  and  $t$ . In addition, the conformity between experimental data and the model predicted values was expressed by both the correlation coefficients ( $R^2$  values close or equal to 1) and adsorption capacities ( $q_e$ ).

In this study, the plot of  $\log(q_e - q_t)$  vs. time  $t$  is not linear over the entire time range as shown in Fig. 5(a), indicating that more than one mechanism is involved in the adsorption process.

Also, from the kinetic data, it was found that the experimental  $q_e$  values (0.09139 for BWGI and 0.0935 meq/g for BWGII) did not agree with the calculated ones  $q_e$  (0.0413 for BWGI and 0.0289 meq/g for BWGII). These confirm that it is not appropriate to use the Lagergren kinetic model to predict the adsorption kinetics for  $\text{Pb}^{2+}$  onto both BWGI and BWGII.

### 3.5.2. Pseudo-second-order kinetic model

Adsorption kinetics were explained by the pseudo-second-order model given by

Ho and McKay [21] as follows:

$$\frac{dq}{dt} = k_2(q_e - q)^2 \quad (5)$$

Integrating Eq. (5) for the boundary conditions  $q = 0$  to  $q = q_t$  at  $t = 0$  to  $t = t$  is simplified as:

$$\frac{t}{q_t} = \frac{1}{k_2 q_e^2} + \frac{t}{q_e} \quad (6)$$

where  $k_2$  (g/mg min) is the rate constant of second-order adsorption determined from the plot of  $t/q_t$  against  $t$ , as shown in Fig. 5(b).

The correlation coefficients  $R^2$  of the pseudo-second-order kinetic model were higher than 0.9919, the adsorption second-order rate constants are found to be 2.4 and 3.47  $\text{min}^{-1}$  for BWGI and BWGII, respectively, and the calculated values of  $q_e$ , fit quit well with  $q_{\text{exp}}$  as shown in Table 5. These confirm that the pseudo-second-order adsorption mechanism is predominant for adsorption of  $\text{Pb}^{2+}$  by both BWGI and BWGII.

### 3.5.3. Elovich kinetic model

The Elovich equation is given as follows [22]:

$$q_t = 1l\beta \ln \alpha\beta + 1l\beta \ln t \quad (7)$$

where  $\alpha$  (mg/g min) is the initial sorption rate,  $\beta$  (g/mg) is related to the extent of surface coverage, and activation energy for chemisorption.

Plot  $q_t$  vs.  $\ln(t)$  to give a linear relationship with a slope of  $(1/\beta)$  and an intercept of  $(1/\beta) \ln \alpha\beta$  (Fig. 6). Fig. 6 shows that the correlation coefficient values are relatively high, indicating that Elovich model is suitable for modeling the adsorption of  $\text{Pb}^{2+}$  ions onto both BWGI and BWGII.

### 3.5.4. Intraparticle diffusion model

This model based on the theory proposed by Weber and Morriss [23] was employed to identify the diffusion mechanism. This theory assumes an empirically based functional relationship, common to most adsorption processes, where uptake varies almost proportionally to  $t^{1/2}$  rather than to the contact time  $t$ . According to this theory:

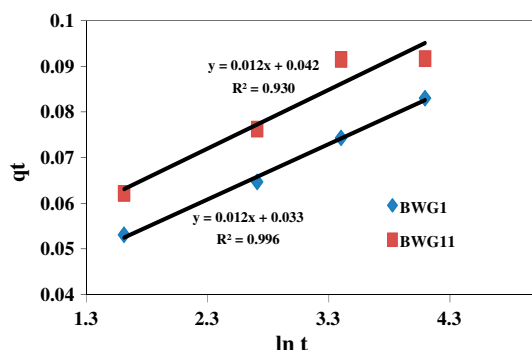
$$q_t = k_{\text{id}} t^{1/2} + C_i \quad (8)$$

where  $k_{\text{id}}$  (mg/g  $\text{min}^{1/2}$ ) is the intraparticle diffusion rate constant, is calculated from the slope of linear portion of  $q_t - t^{1/2}$  plot,  $t^{1/2}$  is the square root of the time, and  $C_i$  (mg/g) is the intercept at stage  $i$ , value of

Table 5

Comparison of the pseudo-first-order and pseudo-second-order adsorption rate constants for  $Pb^{2+}$  onto BWGI and BWGII

Basalt	Pseudo-first-order kinetics			Pseudo-second-order kinetics			$q_{e \text{ exp}}$ (meq/g)
	$q_{e \text{ cal}}$ (meq/g)	$k_1$ ( $\text{min}^{-1}$ )	$R^2$	$q_{e \text{ cal}}$ (meq/g)	$k_2$ (g/mg min)	$R^2$	
BWGI	0.0413	0.0253	0.9919	0.089	2.4	0.9976	0.09139
BWGII	0.0289	0.0532	0.7626	0.097	3.45	0.9984	0.0935

Fig. 6. Elovich kinetic model for  $Pb^{2+}$  adsorption onto BWGI and BWGII.

$C_i$  is related to the thickness of boundary layer i.e. the larger the intercept, the greater the thickness of the boundary layer [24]. The extrapolation of the linear straight lines to the time axis gives intercepts  $C_i$ .

As seen in Fig. 7, the plot of  $q_t$  vs.  $t^{1/2}$  indicates that value of  $C_i = 5.5673$  for BWGI and  $4.413$  mg/g for BWGII. However, if  $C_i \neq 0$ , it indicates that the adsorption process is rather complex and involves more than one diffusive resistance; while, if  $C_i$  is equal to zero, the only controlling step is intraparticle diffusion.

Also, from Fig. 7, the linear line does not pass through the origin, and this deviation from the origin (or near to saturation) might be due to the difference in the mass transfer rate in the initial and final stages of adsorption [25]. The values of the diffusion rate constant  $k_{id}$ ,  $C_i$ , and the regression coefficients  $R^2$  are listed in Table 6.

### 3.6. Effect of adsorbent dose

To optimize the adsorbent dose for the adsorption capacity and  $Pb^{2+}$  removal from aqueous solution, the adsorption of  $Pb^{2+}$  with an initial concentration  $50$  mg/L was conducted using different adsorbent doses ( $0.1$ – $1$  g/100 mL) under the optimum conditions.

Fig. 8 shows that the removal percentage of  $Pb^{2+}$  is increased from  $38$  to  $96\%$  for BWGI ( $0.1$ – $0.9$  g/100 mL)

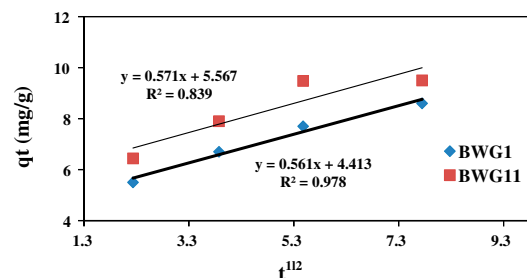
Fig. 7. Intraparticle diffusion model for  $Pb^{2+}$  adsorption onto BWGI and BWGII.

Table 6

The parameters of Intraparticle diffusion model for  $Pb^{2+}$  adsorption onto BWGI and BWGII

Basalt	Intraparticle diffusion model		
	$C_i$	$k_{id}$ ( $\text{mg g}^{-1} \text{min}^{-1/2}$ )	$R^2$
BWGI	4.413	0.561	0.9789
BWGII	5.567	0.571	0.839

and from  $44$  to  $98\%$  for BWGII ( $0.1$ – $0.5$  g/100 mL), respectively. This could be easily explained by an increase in surface area (i.e. due to more availability of active adsorption sites) with an increase in adsorbent dosage. However, several factors affecting adsorption are numbers of sites in the adsorbent material, the accessibility of the sites, the chemical state of sites (i.e. availability), and the affinity between the site and the metal (i.e. binding strength). Therefore, the removal percentage of  $Pb^{2+}$  was remained almost constant from  $0.5$  to  $1$  g/100 mL for BWGI and from  $0.9$  to  $1$  g/100 mL for BWGII [26].

### 3.7. Effect of initial metal ion concentrations and isotherm models

The changes in initial metal concentrations can alter the metal uptake efficiency of an adsorbent through a combination of several factors such as the

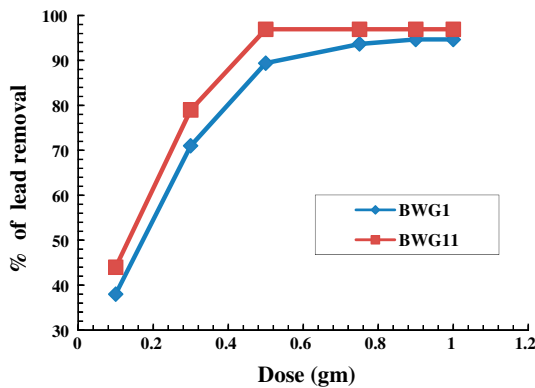


Fig. 8. Effect of adsorbent dose on adsorption of  $Pb^{2+}$  using BWGI and BWGII (volume of solution = 100 mL, concentration of metal ions = 50 mg/L, contact time = 90 min and pH  $5.0 \pm 0.1$ ).

availability of specific surface functional groups and the ability of these groups to bind metal ions [27].

The adsorption percentage decreased from 98.45 to 54.7% for  $Pb^{2+}$  onto BWGI and from 97.55 to 46.5% for  $Pb^{2+}$  onto BWGII. Whereas, increasing the initial metal ion concentration, the driving force of the metal ions toward the active adsorption sites on the adsorbent increases, thus, the amount of metal ion adsorbed per unit mass of the adsorbent increases. On the other hand, at higher metal ion concentrations and the saturation of the available active adsorption sites on the adsorbent surface lead to prevent further metal ion binding hence, the adsorption percentages decrease [27,28].

The equilibrium adsorption isotherms are one of the most important data in order to clarify the mechanism of the adsorption process. Three isotherm models were selected to study the adsorption isotherm, namely Langmuir, Freundlich, and D–R isotherm models. While an adsorption isotherm is characterized by certain constants, which values express the surface properties, the affinity of the adsorbent, and also can be used to find the adsorption capacity of adsorbent.

### 3.7.1. Langmuir isotherm model

This isotherm assumes that adsorption occurs on a homogeneous surface containing sites with equal energy and that are equally available for adsorption. This is valid for the complete monolayer of adsorption, where there is no transportation of adsorbate on the surface plane. This model can be described by non-linear form as follows [29]:

$$q_e = \frac{q_m K_L C_e}{1 + K_L C_e} \quad (9)$$

where  $q_m$  is the maximum adsorption capacity (mg/g), and  $K_L$  is the Langmuir constant (g/L) and is a constant related to the free energy of adsorption as expressed ( $K_L = a e^{-\Delta G/RT}$ ). Deviations from the basic assumption of the Langmuir model do limit interpretation of the values for  $q_m$  and  $K_L$  in terms of absolute surface areas and sorption free energies. The free energy of adsorption,  $\Delta G$  can also be evaluated from the parameter  $K_L$  according to the expression  $\Delta G = -RT \ln K_L$ .

The linear form of Langmuir is given as follows:

$$C_e/q_e = \frac{1}{bq_m} + \frac{1}{q_m} C_e \quad (10)$$

where  $q_e$  (mg/g) is the amount of the metal ions adsorbed per unit mass of adsorbent,  $C_e$  (mg/L) is the equilibrium metal ion concentration in aqueous solution,  $q_m$  (mg/g) and  $b$  (L/mg) are the Langmuir constants related to the adsorption capacity, and free energy or net enthalpy of adsorption, respectively. Thus, a linear plot of  $C_e/q_e$  vs.  $C_e$  confirms the validity of the Langmuir giving correlation coefficients close to unity.

The values of  $q_m$ ,  $b$ , and  $R_L$  are determined from experimental data by linear regression for Langmuir isotherm as shown in Fig. 9 and are presented in Table 7. A further analysis of the Langmuir equation can be made on the basis of a dimensionless equilibrium parameter,  $R_L$  (known as the separation factor) is considered as a more reliable indicator of adsorptions. This parameter ( $R_L$ ) can be expressed by Weber and Chakravorti as follows [30]:

$$R_L = \frac{1}{1 + bC_i} \quad (11)$$

where  $C_i$  is the initial metal ion concentration (mg/L) and  $b$  (L/mg) is the Langmuir constant described

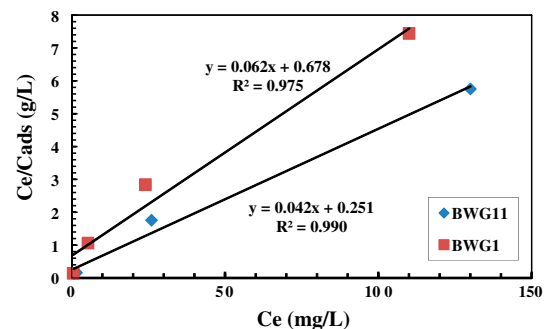


Fig. 9. Langmuir isotherm model for  $Pb^{2+}$  adsorption onto BWGI and BWGII at optimum conditions.

Table 7

Different parameters derived from Langmuir and Freundlich isotherm models for Pb<sup>2+</sup> adsorption onto BWGI and BWGII

Basalt	Langmuir isotherm model			Freundlich isotherm model		
	$q_m$ (mg g <sup>-1</sup> )	$b$ (L mg <sup>-1</sup> )	$R^2$	$K_f$ (mg g <sup>-1</sup> )	$n$	$R^2$
BWGI	16.13	18.95	0.9756	3.615	3.58	0.9378
BWGII	23.8	34.67	0.9901	7.16	4.24	0.9694

above. There are four probabilities for the  $R_L$  value: (i) for favorable adsorption  $0 < R_L < 1$ , (ii) for unfavorable adsorption  $R_L > 1$ , (iii) for linear adsorption  $R_L = 1$ , and (iv) for irreversible adsorption  $R_L = 0$ .

### 3.7.2. Freundlich isotherm model

Freundlich isotherm is an empirical equation that can describe the reversible adsorption onto a heterogeneous surface at sites with different energy of adsorption and is not restricted to the formation of the monolayer of adsorbate. The non-linear form of this model is expressed as follows [31]:

$$q_e = k_f C_e^{1/n} \tag{12}$$

where  $K_f$  is the Freundlich constant (mg/g) and also referred to adsorption capacity, while  $n$  is the heterogeneity factor and related to adsorption intensity. The value of  $n$  can be used to describe the adsorption whether it is linear ( $n = 1$ ), a physical process ( $n > 1$ ) is favorable, or a chemical process ( $n < 1$ ).

On the other hand, the value of  $1/n < 1$  or  $1/n > 1$  indicates a normal Langmuir isotherm and cooperative adsorption, respectively.

Freundlich model can be represented by linear form as follows:

$$\text{Log } q_e = \text{Log } k_f + \text{Log } C_e^{1/n} \tag{13}$$

A plot of  $\text{Log } q_e$  vs.  $\text{Log } C_e$  gives a straight line, where the values of  $K_f$  and  $1/n$  are determined from the intercept and the slope, respectively. (Fig. 10).

From Table 7, the data show that the Langmuir model yields better fit than the Freundlich model.

### 3.7.3. The D–R isotherm model

The D–R isotherm model is used to determine the adsorption type; physical or chemical. The model is given as follows [32]:

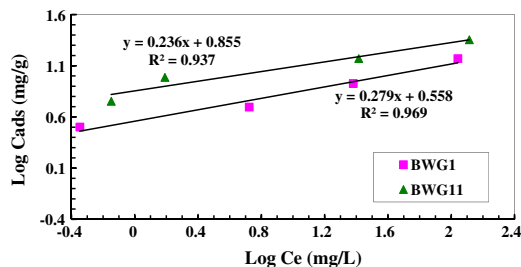


Fig. 10. Freundlich isotherm model for Pb<sup>2+</sup> adsorption onto BWGI and BWGII at optimum conditions.

$$q_e = q_m \exp^{-\beta \epsilon^2} \tag{14}$$

where  $q_e$  (mol/g) is the amount of metal adsorbed onto per unit mass of adsorbent,  $q_m$  (mol/g) is the monolayer adsorption capacity,  $\beta$  (mol<sup>2</sup>k/J<sup>2</sup>) is the activity coefficient related to the mean sorption energy,  $\epsilon$  is the Polanyi potential, and can be calculated from the following equation:

$$\epsilon = RT \ln(1 + 1/C_e) \tag{15}$$

where  $C_e$  (mol/L) is the equilibrium metal ion concentration in aqueous solution. The mean adsorption energy,  $E$  (kJ/mol), can be calculated using the following equation:

$$E = \frac{1}{2\sqrt{-\beta}} \tag{16}$$

The linear form of D–R isotherm model is expressed as:

$$\ln q_e = \ln q_m - \beta \epsilon^2 \tag{17}$$

Fig. 11 shows a plot of  $\ln q_e$  vs.  $\epsilon^2$  to calculate the D–R model constants,  $q_m$  and  $\beta$  from the intercept and slope of linear, respectively.

It was observed that the data obtained from the linear form of D–R isotherm model,  $q_m$  and  $\beta$  were determined from the intercept and slope of linear,

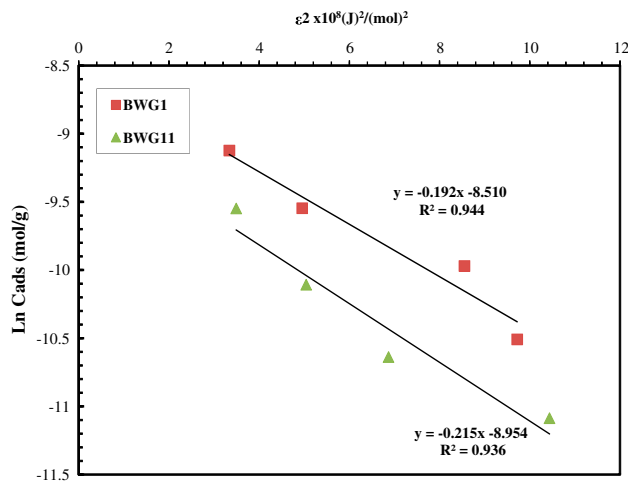


Fig. 11. D–R isotherm model for  $Pb^{2+}$  adsorption onto BWGI and BWGII at optimum conditions.

Table 8

Different parameters derived from Tempkin and the D–R isotherm model for  $Pb^{2+}$  adsorption onto BWGI and BWGII

Basalt	(D–R) isotherm model			
	$q_m$ (mg/g)	$\beta$ ( $mol^2/J^2$ )	$E$ (KJ/mol)	$R^2$
BWGI	$1.29 \times 10^{-4}$	$-0.2153 \times 10^{-8}$	15.24	0.9362
BWGII	$2.013 \times 10^{-4}$	$-0.1922 \times 10^{-8}$	16.13	0.9444

respectively. In addition, the values of free energy were calculated from Eq. (17) and the values of  $E$  were found to be 15.24 and 16.13 kJ/mol for  $Pb^{2+}$  adsorption onto both BWGI and BWGII, respectively. This indicated that the mechanism of  $Pb^{2+}$  adsorption is chemical in nature, and the adsorption process is endothermic (Table 8).

#### 4. Conclusions

The following conclusions are based on the aforementioned findings as follows:

- (i) In this study, it was found that weathering of the basaltic rock improved the adsorption efficiency because the weathering process increased the  $S_{BET}$  surface area and the mean pore radius considerably decreased.
- (ii) The kinetic studies showed that the adsorption of  $Pb^{2+}$  ions onto both BWGI and BWGII (classified by engineering and geological investigation) followed to the pseudo-second-

order model. Therefore, the applicability of this model showed that sorption process is complex and involves more than one mechanism. Furthermore, the intraparticle diffusion model, the value of  $C_i \neq 0$ , indicated that the adsorption process is rather complex and involves more than one diffusive resistance.

- (iii) The adsorption isotherm data for the adsorption of  $Pb^{2+}$  ions were fitted well to the Langmuir model. From Langmuir model equations, the maximum adsorption capacities were found to be 15.92 and 23.31 mg/g for  $Pb^{2+}$  adsorptions on both BWGI and BWGII, respectively. Between 25 and 200 mg/L of initial  $Pb^{2+}$  concentration, the  $R_L$  values ranged from 0.0021 to 0.001 for BWGI and from 0.001 to 0.00014 for BWGII, then approached zero with increase in the  $C_i$  values of  $Pb^{2+}$ , indicating that  $Pb^{2+}$  adsorption onto basalt is highly favorable under studied conditions. The mean sorption energy ( $E$ ), obtained from D–R isotherm model, indicated that the adsorption mechanism is chemical in nature and the reaction is endothermic.
- (iv) The present investigation proved that the basaltic rock can be used as a low cost and an effective adsorbent for the removal of  $Pb^{2+}$  ions from aqueous solutions and hence, its applicability to remove  $Pb^{2+}$  from wastewater is expected to be economically feasible.

#### References

- [1] P. Amiotte Suchet, J.-L. Propst, W. Ludwig, worldwide distribution of continental rock lithology: Implications for atmospheric/soil  $CO_2$  uptake by continental weathering and alkalinity river transport to the oceans Glob. Biogeochem. Cycl. 17 (2003) 7.1–7.13.
- [2] M.K. Saunders, P.G. Fookes, A review of the relationship of rock weathering and climate and its significance to foundation engineering, Eng. Geol. 4 (1970) 289–325.
- [3] S.I. Tomkeieff, The basalt lavas of the Giant's Causeway district of Northern Ireland, Bull. Volcan. 6 (1940) 89–143.
- [4] A. Spry, The origin of columnar jointing, particularly in basalt flows, J. Geol. Soc., Australia, 8 (1962) 191–216.
- [5] N.N. Souza, Jr, 'Entablamento' em Derrames Basálticos da Bacia do Parani: Aspectos Genético e Caracterização Geotécnica (Aspectos Genético e Caracterização Geotécnica), Tese (Doutorado) (Thesis (Ph.D.)), Escola de Engenharia de So Carlos (School of Engineering of So Carlos) - USP, 1992, p. 257.
- [6] P.E. Long, B.J. Wood, Structures, textures, and cooling histories of Columbia River basalt flows, Geol. Soc. Am. Bull. 97 (1986) 1144–1155.

- [7] J.H. Potgieter, S.S. Potgieter-Vermaak, P.D. Kalibantonga, Heavy metals removal from solution by palygorskite clay, *Miner. Eng.* 19 (2006) 463–470.
- [8] M. Eloussaief, M. Benzina, Efficiency of natural and acid-activated clays in the removal of Pb(II) from aqueous solutions, *J. Hazard. Mater.* 178 (2010) 753–757.
- [9] H. Aydın, Y. Bulut, Ç. Yerlikaya, Removal of copper (II) from aqueous solution by adsorption onto low-cost adsorbents, *J. Environ. Manage.* 87 (2008) 37–45.
- [10] A. Roads, A catalyst for development, *Municipal Engineer* 26 (1995) 35–37.
- [11] A.S. Gupta, K.S. Rao, Index properties of weathered rocks: Inter-relationships and applicability, *Bull. Eng. Geol. Env.* 57 (1998) 161–172.
- [12] Standard Methods for the Examination of Water & Wastewater, twenty-second ed., American Public Health Association (APHA), American Water Works Association (AWWA) & Water Environment Federation (WEF), 2012.
- [13] G. Annadurai, R.S. Juang, D.J. Lee, Adsorption of heavy metals from water using banana and orange peels, *Water Sci. Tech.* 47 (2003) 185–190.
- [14] K.G. Cox, J.D. Bell, R.J. Pankhurst, *The Interpretation of Igneous Rocks*, George Allen and Unwin, London, 1979, p. 450.
- [15] P.N.W. Verhoef, A.R.G. Van de Wall, Application of petrography in durability assessment of rock construction materials, in: Balkema (Ed.), *Aggregate Resources*, 1998, pp. 307–330.
- [16] IPT (Instituto de Pesquisas Tecnológicas do Estado de São Paulo), *Characteristics Tecnologicas das Rochas Ornamentais Utilizadas como Materiais de Como Materiais de Construç Civil do Estado de So Paulo*, 1980 (IPT, relation, 14.710).
- [17] D. Mohan, K.P. Singh, Single- and multi-component adsorption of cadmium and zinc using activated carbon derived from bagasse—An agricultural waste, *Water. Res.* 36 (2002) 2304–2318.
- [18] M.Q. Jiang, X.Y. Jin, X.O. Lu, Z.L. Chen, Adsorption of Pb(II), Cd(II), Ni(II) and Cu(II) onto natural kaolinite clay, *Desalination* 252 (2010) 33–39.
- [19] H.S. Ibrahim, A.A. El-Kady, N.S. Ammar, L. Meesuk, P. Wathanakul, M.A. Abdel-Wahhab, Application of isotherm and kinetic models for the removal of lead ions from aqueous solutions, *J. Environ. Eng.* 139 (2013) 349–357.
- [20] S. Lagergren, Zur Theorie der sogenannten Adsorption gelöster Stoffe (On the theory of so-called adsorption of solutes), *K. Sven. Vetenskapsakad. Handl.* 24 (1898) 1–39.
- [21] Y.S. Ho, G. McKay, Sorption of dye from aqueous solution by peat, *Chem. Eng. J.* 70 (1998) 115–124.
- [22] C.W. Cheung, J.F. Porter, G. Mckay, Sorption kinetic analysis for the removal of cadmium ions from effluents using bone char, *Water Res.* 35 (2001) 605–612.
- [23] W.J. Weber, J.C. Morriss, Kinetics of adsorption on carbon from solution, *J. Sanitary Eng. Div. Am. Soc. Civ. Eng.* 89 (1963) 31–60.
- [24] M. Sathishkumar, A.R. Binupriya, D. Kavitha, R. Selvakumar, R. Jayabalan, J.G. Choi, S.E. Yun, Adsorption potential of maize cob carbon for 2,4-dichlorophenol removal from aqueous solutions: Equilibrium, kinetics and thermodynamics modeling, *Chem. Eng. J.* 147 (2009) 265–271.
- [25] I.A.W. Tan, A.L. Ahmad, B.H. Hameed, Adsorption of basic dye on high-surface area activated carbon prepared from coconut husk: Equilibrium, kinetic and thermodynamic studies, *J. Hazard. Mater.* 154 (2008) 337–346.
- [26] A. Agrawal, K.K. Sahu, B.D. Pandey, Removal of zinc from aqueous solutions using sea nodule residue, *Colloids Surf., A* 237 (2004) 133–140.
- [27] V.O. Arief, K. Trilestari, J. Sunarso, N. Indraswati, S. Ismadji, Recent progress on biosorption of heavy metals from liquids using low cost biosorbents: Characterization, biosorption parameters and mechanism studies, *Clean* 36 (2008) 937–962.
- [28] M. Jiang, X. Jin, X.-Q. Lu, Adsorption of Pb(II), Cd(II), Ni(II) and Cu(II) onto natural kaolinite clay, *Desalination* 252 (2010) 33–39.
- [29] I. Langmuir, The adsorption of gases on plane surfaces of glass, mica and platinum, *J. Am. Chem. Soc.* 40 (1918) 1361–1403.
- [30] T.W. Weber, R.K. Chakravorti, Pore and solid diffusion models for fixed bed adsorbents, *AIChE J.* 20 (1974) 228–238.
- [31] H.M.F. Freundlich, Über die adsorption in Lösungen (Over the adsorption in solutions), *Z. Phys. Chem.* 57 (1906) 385–470.
- [32] M.M. Dubinin, L.V. Radushkevich, Equation of the characteristics curve of activated charcoal, *Chem. Zent.* 1 (1947) 875.